Transp Porous Med
DOI 10.1007/s11242-010-9584-x

Thermal Analysis of Flow in a Porous Medium Over a Permeable Stretching Wall

A. Tamayol · K. Hooman · M. Bahrami

Received: 1 December 2009 / Accepted: 8 April 2010

Abstract This work presents a similarity solution for boundary layer flow through a porous medium over a stretching porous wall. Two considered wall boundary conditions are power-law distribution of either wall temperature or heat flux which are general enough to cover the isothermal and isoflux cases. In addition to momentum, both first and second laws of thermodynamics analyses of the problem are investigated. Independent numerical simulations are also performed for verification of the proposed analytical solution. The results, from the two independent approaches, are found to be in complete agreement. A comprehensive parametric study is presented and it is shown that heat transfer and entropy generation rates increase with Reynolds number, Prandtl number, and suction to the surface.

Keywords Similarity solution · Wall suction/injection · Stretching surface · Entropy generation · Boundary layer · Porous media

List of Symbols

Be	Bejan number, Eq. 24
f	Similarity function for velocity
f_w	Injection parameter, $f_w = -v_w L/u_0\sqrt{K}$
K	Permeability, m^2
L	Stretching surface length, m
n	Power of temperature/heat flux distribution
Nu	Local Nusselt number

A. Tamayol (✉) · M. Bahrami
Mechatronic Systems Engineering, School of Engineering Science, Simon Fraser University, Surrey, BC V3T 0A3, Canada
e-mail: ali_tamayol@sfu.ca

K. Hooman
School of Mechanical and Mining Engineering, The University of Queensland, Brisbane, QLD 4072, Australia

Published online: 20 May 2010

Nu_L	Averaged Nusselt number
Pr	Prandtl number, $Pr = \nu/\alpha_{eff}$
q_0	Wall heat flux coefficient, W/m^2
Re	Reynolds number, $Re = \rho u_0 K/L$
S_{gen}	Entropy generation rate, N/K m^2 s
T	Temperature, K
T_0	Wall temperature coefficient, K
u	Velocity in x-direction, m/s
u_0	Wall velocity coefficient, m/s
v	Velocity in y-direction, m/s
v_w	Injection velocity, m/s
x	Coordinate system, m
y	Coordinate system, m

Greek Symbols

α_{eff}	Effective thermal diffusivity, m^2/s
η	Similarity parameter, $\eta = y/\sqrt{K}$
θ	Similarity function for temperature
κ	Thermal conductivity, W/mK
μ	Viscosity, N s/m^2
μ_{eff}	Effective viscosity, N s/m^2
ν	Kinematic viscosity, m^2/s
τ_w	Wall shear stress, N/m^2
τ_L	Averaged wall shear stress, N/m^2
ψ	Stream function, m^2/s

1 Introduction

The study of boundary layers over a stretching surface has application in several engineering processes such as liquid composite molding, extrusion of plastic sheets, paper production, glass blowing, metal spinning, wire drawing, and hot rolling (Yu et al. 2000; Al-Odat et al. 2006; Nazar et al. 2008). More importantly, the quality of the products, in the above-mentioned processes, depends on the kinematics of stretching and the simultaneous heat and mass transfer rates during the fabrication process.

Sakiadis (1961a, b) and Crane (1970) were the pioneers in the investigations of boundary layer flow over continuously moving surfaces that are quite different from the free stream flow over stationary flat plates. The flow field of a stretching surface with a power-law velocity variation was discussed by Banks (1983). Furthermore, a stretching surface subject to suction or injection was studied by Ali (1995) for uniform and variable surface temperatures while Elbashbeshy (1998) investigated the uniform and variable surface heat flux. Recently, analytical solution for velocity distribution inside a porous medium with a stretching boundary is published by Pantokratoras (2009). Magyari and Keller (2000) have analyzed the exponential stretching problem by discussing a similarity solution of momentum and energy equations. Unsteady heat transfer over a stretching surface is studied by Elbashbeshy and Bazid (2004) and Mehmood et al. (2008). Seshadri et al. (1995) investigated non-Newtonian fluid flow effects on the hydrodynamic field over a stretching surface subjected to mass transfer.

Effects of various heat transfer modes on the velocity and temperature fields over stretching surfaces are studied by (Kumari et al. 1996; Ishak et al. 2006; Elbashbeshy and Bazid 2000). Kumari et al. (1996) reported the unsteady free convection flow over a continuous moving vertical surface while Ishak et al. (2006) theoretically investigated the unsteady mixed convection boundary layer flow and heat transfer from a stretching vertical surface in a quiescent viscous and incompressible fluid. Later, employing a similarity solution technique, Elbashbeshy and Bazid (2000) included thermal radiation effects in a stretching surface problem.

Porous materials can be used to enhance the heat transfer rate from stretching surfaces to improve processes such as hot rolling and composite fabrication (Tamayol and Bahrami 2009). Elbashbeshy and Bazid (2000) analysed the flow of a variable-viscosity fluid through a porous medium over a stretching surface. Heat transfer in a porous medium with internal heat generation was also studied by Elbashbeshy and Bazid (2003). This work was extended by Cortell (2005) to include power-law temperature distribution.

In all of the above studies, the goal was to understand the flow behavior in order to minimize the losses of the system. As the destroyed exergy, available work of the system, is linearly proportional to the generated entropy (Bejan 1995), it makes perfect engineering sense to study and minimize the entropy generation of the system which is commonly referred to as entropy generation minimization (EGM), as an optimization tool (Bejan et al. 2004).

A quick review of literature shows that, in spite of numerous studies on the stretching surface problem, a second law analysis of heat transfer from a permeable stretching surface is not yet available. In addition, the heat flux boundary condition is not investigated thoroughly in the literature. Moreover, the reported similarity solutions (obtained after simplifications) are not verified through comparison with numerical or experimental results with the exception of Kiwan and Ali (2008).

In view of the above, a similarity solution is developed in the present study to solve fluid flow, heat transfer, and entropy generation in a porous medium over a porous plate with linear velocity, subjected to different power-law thermal boundary conditions. The analytical solution is successfully validated in comparison with numerical analysis.

2 Problem Statement

A steady, constant properties, two-dimensional flow through a homogenous porous medium of permeability K, over a stretching surface with linear velocity distribution, i.e., $u_w = u_0 x/L$ is assumed (see Fig. 1). The transport properties of the medium can be considered independent of temperature when the difference between wall and ambient temperatures are not significant (Kaviany 1992). The origin is kept fixed while the wall is stretching and the y-axis is perpendicular to the surface. Using the above-mentioned assumptions, the continuity equation is (Kaviany 1992):

$$\frac{\partial u}{\partial x} + \frac{\partial v}{\partial y} = 0 \tag{1}$$

where u and v are velocity components in the x and y directions, respectively. The Brinkman model x-momentum equation reads (Nield and Bejan 2006):

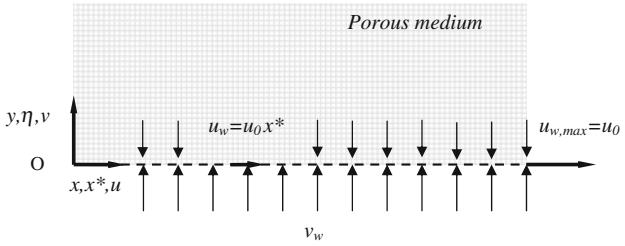

Fig. 1 Schematic of the problem geometry

$$\rho\left(u\frac{\partial u}{\partial x}+v\frac{\partial u}{\partial y}\right)=\mu_{\text{eff}}\frac{\partial^2 u}{\partial y^2}-\frac{\mu}{K}u, \tag{2}$$

where μ_{eff} is the effective viscosity (Brinkman 1949; Kaviany 1992) which for simplicity in the present study is considered to be identical to the dynamic viscosity, μ. This assumption is reasonable for packed beds of particles (Starov and Zhdanov 2001). It should be noted that the proposed approach can easily be extended to the general case. The transport properties of the porous medium such as permeability depends on its microstructure and can be calculated either using existing correlations in the literature or through experimental measurements (Kaviany 1992; Tamayol and Bahrami 2009). The energy equation is based on local thermal equilibrium that hypothesizes the solid and fluid phases are at the same temperature at each point in the medium (Nield and Bejan 2006). After neglecting the small terms due to thin thermal boundary layer thickness, the energy equation becomes:

$$u\frac{\partial T}{\partial x}+v\frac{\partial T}{\partial y}=\alpha_{\text{eff}}\frac{\partial^2 T}{\partial y^2}, \tag{3}$$

where α_{eff} is the effective thermal diffusivity of the medium (Nield and Bejan 2006; Sadeghi et al. 2008). The hydrodynamic boundary conditions are:

$$u(x^*,0)=u_0x^*,\quad v(x^*,0)=v_w,\quad u(x^*,\infty)=0, \tag{4}$$

where $x^*=x/L$ is the non-dimensional x-coordinate and L is the length of the porous plate. The following thermal boundary conditions are considered:

$$T(x^*,0)=T_\infty+T_0\left(x^*\right)^n,\quad T(x^*,\infty)=T_\infty \tag{5}$$

$$-\kappa\left.\frac{\partial T}{\partial y}\right|_{(x^*,0)}=q_0\left(x^*\right)^n,\quad T(x^*,\infty)=T_\infty, \tag{6}$$

where κ is the effective thermal conductivity of the medium and is a function of thermal conductivities of the fluid and solid phases and the porous medium microstructure (Kaviany 1992; Nield and Bejan 2006; Sadeghi et al. 2008). The power-law temperature and heat flux distribution, described in Eqs. 5 , 6, present a wider range of thermal boundary conditions including isoflux and isothermal cases. For example, by setting n equal to zero, Eqs. 5, 6 yield isothermal and isoflux, respectively.

Second law of thermodynamics analysis of porous media is found to be more complicated compared to the clear fluid counterpart due to increased number of variables in governing equations (Hooman and Gurgenci 2007). In the non-Darcian regime, there are three alternative models for the fluid friction term being the clear-fluid compatible model, the Darcy model, and the Nield model or the power of drag model; see (Hooman et al. 2007) for more details. In a recent study, Hooman and Gurgenci (2007) have compared these three models

and concluded that they are effectively identical for low values of permeability. Following the entropy generation function introduced by Hooman et al. (2007), the volumetric entropy generation rate, S_{gen}, reads:

$$S_{\text{gen}} = \frac{\kappa}{T^2}\left[\left(\frac{\partial T}{\partial x}\right)^2 + \left(\frac{\partial T}{\partial y}\right)^2\right] + \frac{\mu}{T}\left\{2\left[\left(\frac{\partial u}{\partial x}\right)^2 + \left(\frac{\partial v}{\partial y}\right)^2\right] + \left(\frac{\partial u}{\partial y} + \frac{\partial v}{\partial x}\right)^2\right\} + \frac{\mu}{TK}\left(u^2 + v^2\right) \tag{7}$$

Using boundary layer approximations (Nield and Bejan 2006), Eq. 7 reduces to:

$$S_{\text{gen}} = \frac{\kappa}{T^2}\left(\frac{\partial T}{\partial y}\right)^2 + \frac{\mu}{T}\left(\frac{\partial u}{\partial y}\right)^2 + \frac{\mu}{TK}\left(u^2\right) \tag{8}$$

3 Similarity Solution

Similarity solution is a classical approach in analyzing boundary layer problems, details of which are available in the literature, for applications of this technique to convection in porous media (see Kaviany 1992; Nield and Bejan 2006).

3.1 Hydrodynamics

Using the stream function, $\psi(x, y)$, the continuity equation is satisfied:

$$u = \frac{\partial \psi}{\partial y}, \quad v = -\frac{\partial \psi}{\partial x} \tag{9}$$

According to Nield and Kuznetsov (2005), the hydrodynamic boundary layer thickness scales with $\sqrt{K}$. This can be found through a scale analysis between the first and the second terms on the right hand side of Eq. 2, i.e., the viscous and the Darcy terms. Therefore, instead of the other similarity parameters reported in the literature, the following dimensionless similarity parameter is defined:

$$\eta = \frac{y}{\sqrt{K}} \tag{10}$$

The u-velocity is assumed to be correlated to $f(\eta)$, a dimensionless similarity function as:

$$u = u_0 x^* f'(\eta) \tag{11}$$

where f' is $\mathrm{d}f/\mathrm{d}\eta$. Using stream function definition, Eq. 9, the stream function and the v-velocity take the following form:

$$v = -\frac{u_0}{L}\sqrt{K} f(\eta), \quad \psi = u_0 x^* \sqrt{K} f(\eta) \tag{12}$$

Substituting for u and v into Eqs. 2, 4, one will find the following differential equation for the u-momentum equation:

$$f''' + Re(ff'' - f'^2) - f' = 0, \quad Re = \frac{\rho u_0 K}{L\mu}, \tag{13}$$

where Re is the Reynolds number. Equation 13 should be solved subject to the following boundary conditions:

$$f'(0) = 1, \quad f(0) = -\frac{v_w L}{u_0 \sqrt{K}} = f_w, \quad f'(\infty) = 0 \tag{14}$$

f_w is the injection parameter. Positive/negative values of f_w show suction/injection into/from the porous surface, respectively. The exact solution of Eq. 13 with the boundary conditions given in Eq. 14 is:

$$f = f_w + \frac{1 - e^{(-\gamma \eta)}}{\gamma}, \quad \gamma = \frac{Ref_w + \sqrt{(Ref_w)^2 + 4\,(Re + 1)}}{2} \tag{15}$$

The wall shear stress is the driving force that drags fluid flow along the stretching wall. The wall shear stress term can then be found, in terms of the similarity function, as

$$\tau_w = -\mu \left.\frac{\partial u}{\partial y}\right|_{y=0} = \frac{-\mu u_0\, x^* f''(0)}{\sqrt{K}} \tag{16}$$

Taking the average over the plate length, we have:

$$\tau_L = \frac{-\mu u_0\, L f''(0)}{2\sqrt{K}} \tag{17}$$

3.2 Thermal Analysis

Introducing a similarity function, θ, as:

$$T - T_\infty = T_{ref} \left(x^*\right)^n \theta(\eta), \tag{18}$$

where T_{ref} is T_0 and $q_0\sqrt{K}/\kappa$ for the power-law temperature and heat flux boundary conditions, respectively. The thermal energy equation reads:

$$\theta'' + Re \cdot Pr(f\theta') - n \cdot Re \cdot Pr(f'\theta) = 0 \tag{19}$$

and is subjected to the following boundary conditions:

$$\theta(0) = 1, \quad \theta(\infty) = 0 \qquad \text{Power-law temperature} \tag{20a}$$

$$\theta'(0) = -1, \quad \theta(\infty) = 0 \qquad \text{Power-law heat flux} \tag{20b}$$

for power-law temperature and heat flux boundary conditions, respectively. Employing the definition of convective heat transfer coefficient, the local Nusselt numbers, become:

$$Nu_x = \frac{hx}{\kappa} = \begin{cases} -\frac{\theta'(0)x}{\sqrt{K}} & \text{Power-law temperature} \\ \frac{q_w x}{\kappa(T_w - T_\infty)} = \frac{x}{\theta(0)\sqrt{K}} & \text{Power-law heat flux} \end{cases} \tag{21}$$

The average Nusselt numbers, then take the following forms:

$$Nu_L = \frac{hL}{\kappa} = \begin{cases} -\frac{\theta'(0)L}{2\sqrt{K}} & \text{Power-law temperature} \\ \frac{L}{2\theta(0)\sqrt{K}} & \text{Power-law heat flux} \end{cases} \tag{22}$$

Finally, the local volumetric entropy generation rate for the above cases, respectively, read:

$$S_{\text{gen}} = \frac{\kappa}{\left(\theta T_0 \left(x^*\right)^n + T_\infty\right)^2}\left(\frac{\theta' T_0 \left(x^*\right)^n}{\sqrt{K}}\right)^2 + \frac{\mu}{\left(\theta T_0 \left(x^*\right)^n + T_\infty\right)} \times \left[\left(\frac{f'' u_0 x^*}{\sqrt{K}}\right)^2 + \left(\frac{f' u_0 x^*}{\sqrt{K}}\right)^2\right] \tag{23a}$$

$$S_{\text{gen}} = \frac{\kappa}{\left(\theta\sqrt{K} q_0 \left(x^*\right)^n/\kappa + T_\infty\right)^2}\left(\frac{\theta' q_0 \left(x^*\right)^n}{k}\right)^2 + \frac{\mu}{\left(\theta\sqrt{K} q_0 \left(x^*\right)^n/\kappa + T_\infty\right)} \times \left[\left(\frac{f'' u_0 x^*}{\sqrt{K}}\right)^2 + \left(\frac{f' u_0 x^*}{\sqrt{K}}\right)^2\right] \tag{23b}$$

4 Numerical Simulation

Commercially available software CFD-ACE (ESI Software) is used, similar to (Famouri and Hooman 2008; Hooman 2008), to solve the set of momentum and energy equations, Eqs. 1–3 subject to the aforementioned boundary conditions, Eqs. 4–6. The computational domain, a rectangular box (1×10; dimensionless), was generated with triangular grids using the commercial package CFD-GEOM (ESI Software) that is typically used in conjunction with the commercially available finite volume flow solver CFD-ACE.

Grids were controlled in CFD-GEOM using curvature criterion, transition factor, and maximum and minimum cell sizes. For each case these values were 30°, 1.1, 0.01, and 0.00003, respectively. The maximum cell size is still smaller than the expected size of the boundary layer thickness (Hooman 2008) for $K = 10^{-3}$ m^2. This combination has lead to 29,414 cells. Grid-independence was tested by control runs on a finer grid with 49,526 cells that produced consistent results (with a maximum error of $<2\%$). The results, as will be shown later, are in good agreement with those of similarity solution as depicted by Fig. 2. Hence, finer grids were not used in reporting the results. It should be noted that the convergence criterion, maximum relative error in the values of the dependent variables between two successive iterations, in all runs was set at 10^{-5}.

5 Results and Discussion

The governing equations and their boundary conditions are transformed to ordinary differential equations which are solved numerically using the fourth order Runge–Kutta integration scheme featuring a shooting technique. This means that $\theta'(0)$ or $\theta(0)$, depending on the considered boundary condition, are assumed and the results at $\eta \to \infty$ are checked. If the boundary conditions at infinity are not satisfied, the presumed values should be modified. Elbashbeshy and Bazid (2003) reported that applying the infinity boundary conditions at $\eta = 10$ is sufficiently far. Hence, in the present study the infinity boundary condition is applied at $\eta = 10$.

The non-dimensional numbers introduced in the present analysis are Reynolds number, Re, Prandtl number, Pr, and the injection number, f_{w}. Another important parameter is the power of the surface temperature/heat flux distribution, n, which is considered in this study.

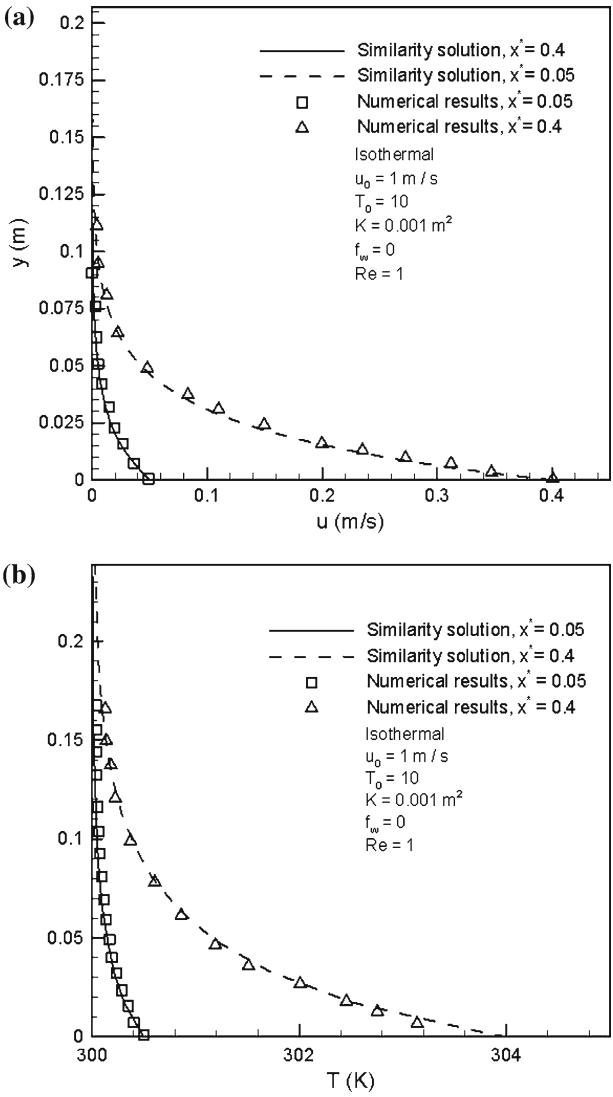

Fig. 2 **a** Velocity and **b** temperature profiles in various locations for $Re = 1$, $f_w = 0$, $K = 0.001$ m^2, $T_0 = 10°$C, $n = 0$, $Pr = 1$, and $u_0 = 1$ m/s

Effect of Reynolds number variation on velocity and temperature distribution is investigated as depicted in Fig. 3. As expected, by increasing the Reynolds number, viscous forces become less important; thus, the velocity defects in the flow field will less propagate. The predicted values of the non-dimensional viscous and thermal boundary layer thicknesses, η_v and η_T, are reported in Fig. 4; these values are in line with this observation. η_v and are the distances from the surface that velocity and temperature defects are 1% of the wall values. Plotted values of Nu_L and τ_w for different Reynolds numbers in Fig. 5 have reverse and direct relationships with Re. Note that for higher Reynolds numbers less fluid is dragged with surface; therefore, the wall shear stress is reduced.

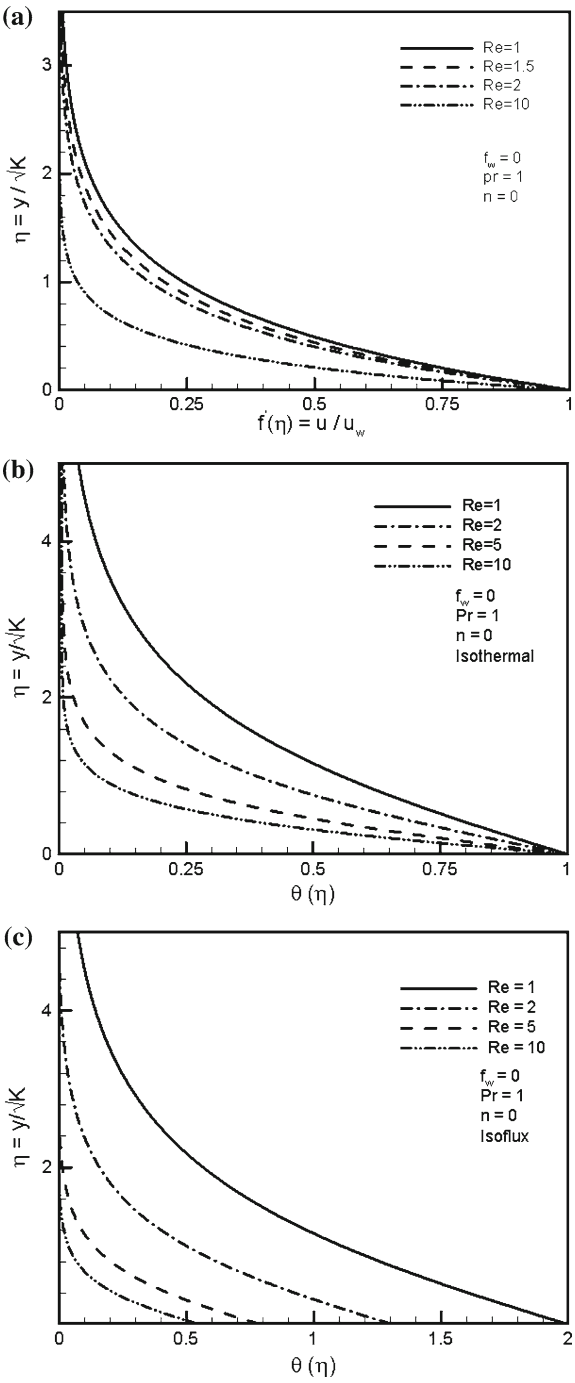

Fig. 3 Effects of *Re* on velocity and temperature profiles with different boundary conditions

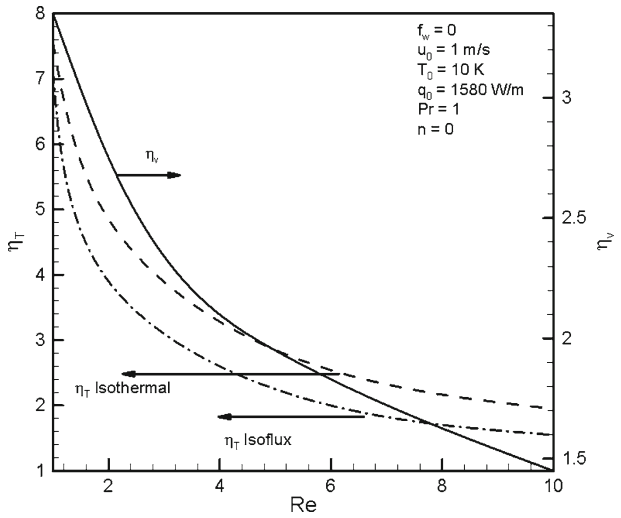

Fig. 4 Effect of Reynolds number on velocity and temperature boundary layer thicknesses

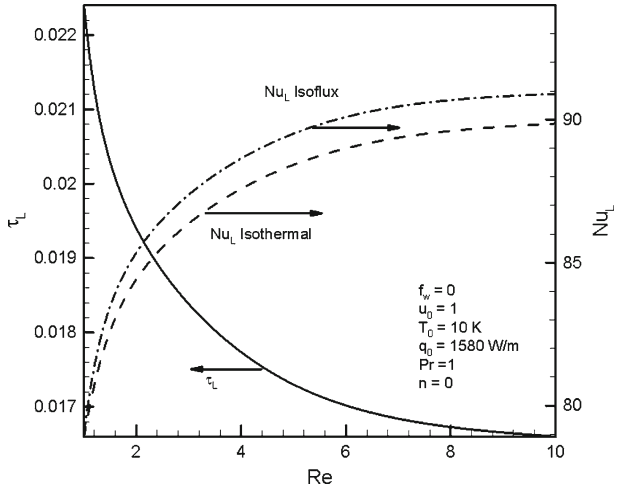

Fig. 5 Effects of Reynolds number on wall shear stress and averaged Nusselt number

Suction or injection from the stretching surface affects the boundary layer thicknesses; hence, it alters the shear drag and heat transfer rate of the surface. Figure 6 is presented to investigate the effects of f_w on velocity and temperature profiles. As shown, all boundary layer thicknesses decrease as f_w increases from negative (injection) to positive (suction) values. As a result, the wall sheer stress and the averaged Nusselt number increase with f_w as shown in Fig. 7.

Prandtl number provides an estimation for the ratio of η_v and η_T. Therefore, for a constant viscous boundary layer, η_T increases with Pr; this is shown in Fig. 8. Consequently, Nu_L has a direct relationship with Pr, see Fig. 8.

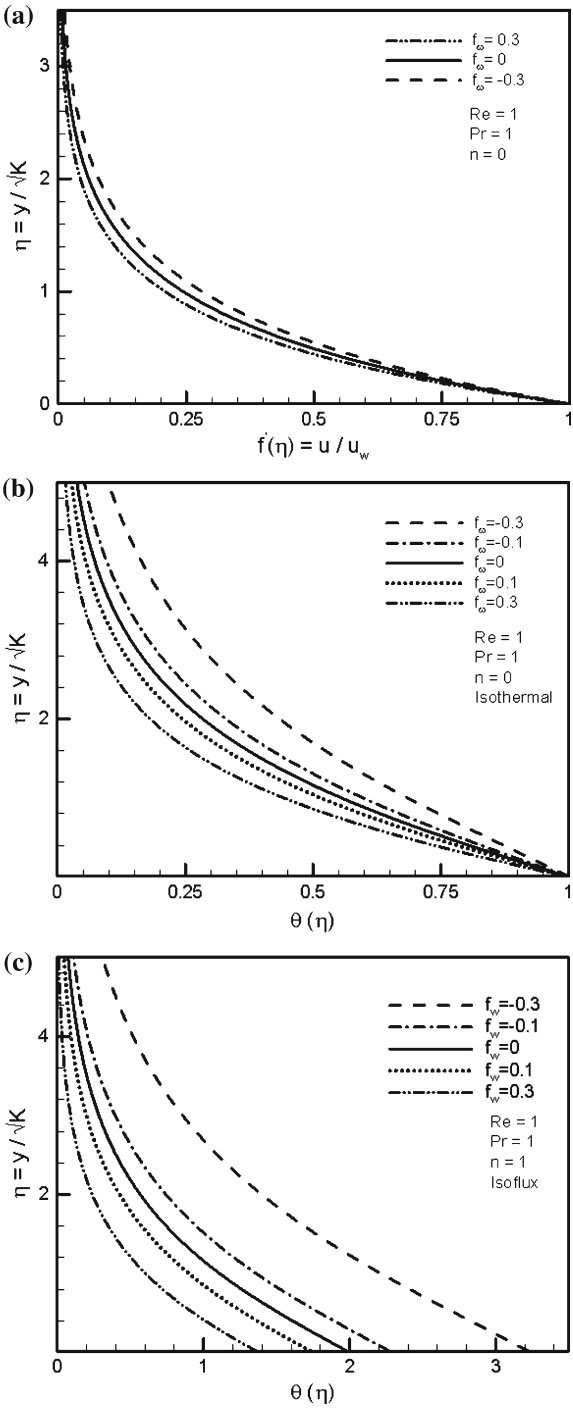

Fig. 6 Effects of wall injection/suction parameter on velocity and temperature profiles for different boundary conditions

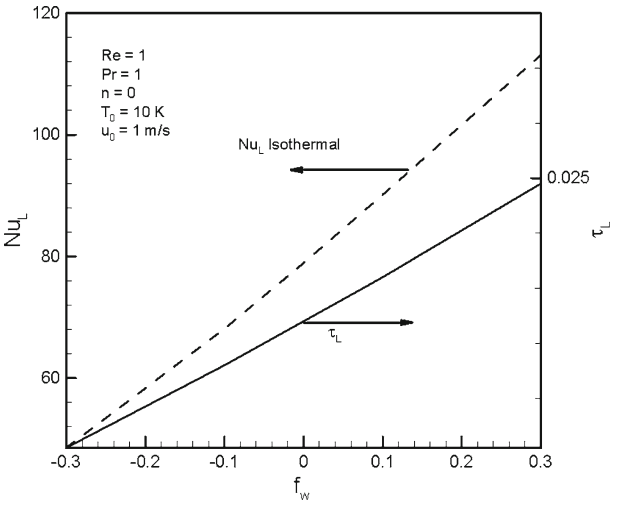

Fig. 7 Effects of suction/injection parameter on wall shear stress and averaged Nusselt number

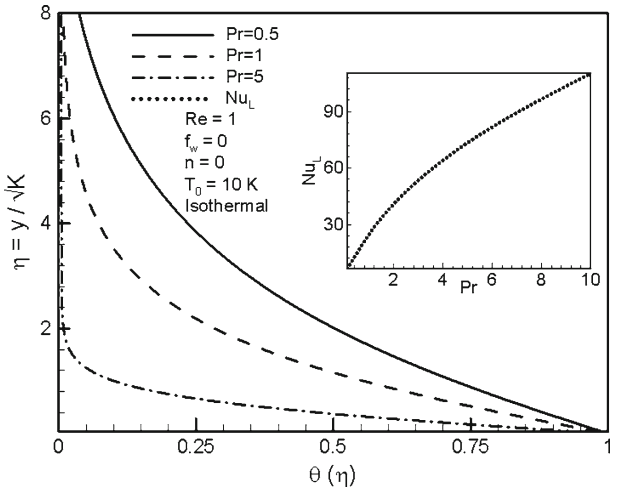

Fig. 8 Effects of Prandtl number on temperature distribution and Nu_L

Figure 9 shows the effect of n on the temperature field for both types of the thermal boundary conditions considered here. Increasing n reduces the thermal boundary layer thickness regardless of the boundary condition type leading to a heat transfer augmentation.

Entropy generation rate and Bejan number are investigated in Figs. 10, 11, and 12. The Bejan number, Be, is defined as:

$$Be = \frac{\text{Entropy generation due to heat transfer}}{\text{Total entropy generation}} \tag{24}$$

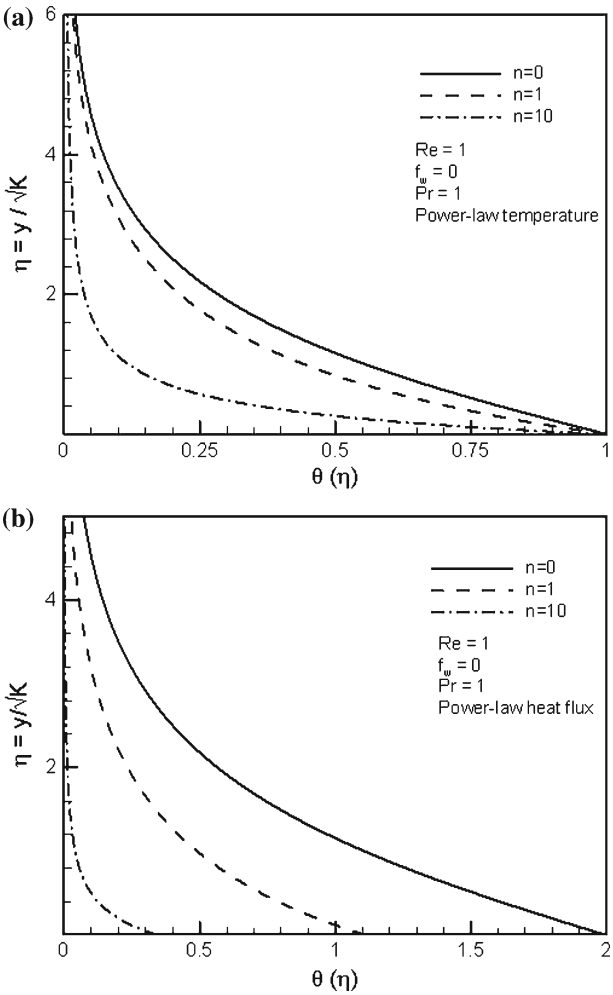

Fig. 9 Effects of *n* on similarity temperature distribution of power-law: **a** temperature and **b** heat flux boundary condition

Bejan number ranges from 0 to 1 and when the entropy generation due to heat transfer is dominant and Be is close to 1. As shown in Fig. 10, both the entropy generation rate and Be increase with Reynolds number. The reason is that the heat transfer rate between two energy sources with different temperature increases with Re. Wall suction also increases surface heat transfer rate; thus, results in higher S_{gen} and Be; Figure 11 shows the same trend. Calculated values for entropy generation rate for different values of Pr are plotted in Fig. 12. As expected increasing the Prandtl number results in entropy generation augmentation.

6 Summary and Conclusions

Wall driven flow through a porous medium over a stretching permeable surface subjected to power-law temperature and heat flux boundary conditions are studied. Similarity solution

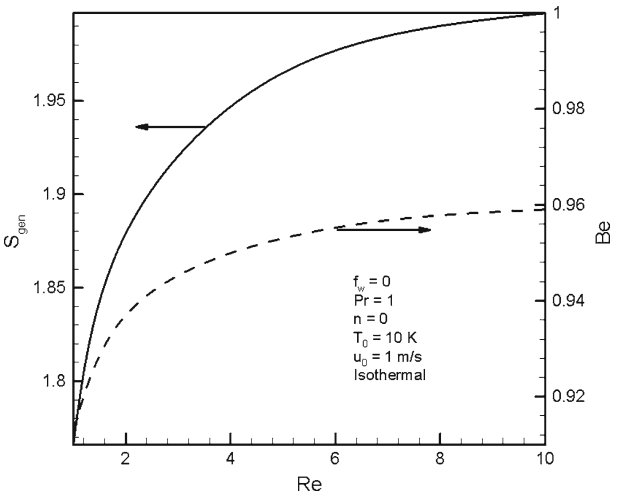

Fig. 10 Effect of Reynolds number on entropy generation rate and Bejan number

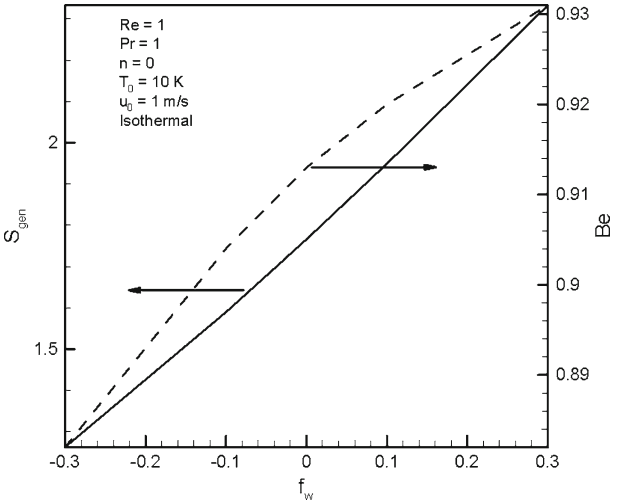

Fig. 11 Effect of injection parameter on entropy generation rate and Bejan number

technique is employed and boundary layer equations are transformed to ordinary differential equations and solved numerically. The accuracy of this method is verified through comparison of the results with CFD simulations. Introducing non-dimensional numbers, a parametric study is performed. Moreover, second law (of thermodynamics) aspects of the problem are investigated. The highlights of this study are:

– The non-dimensional viscous boundary layer thickness has a direct relationship with Reynolds number; thus Nusselt number and entropy generation rate increases with Re.
– Nusselt number, wall shear stress, and entropy generation rate have a reverse relationship with and mass transfer from the wall, f_w.

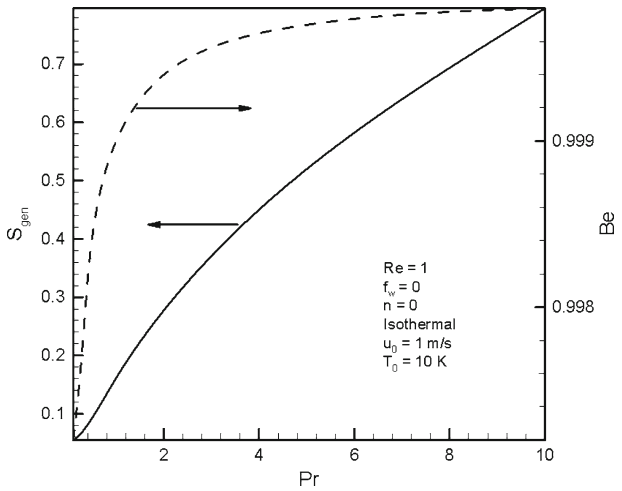

Fig. 12 Effect of Prandtl number on entropy generation rate and Bejan number

– Increasing the Prandtl number results in reduction of thermal boundary layer thickness. Consequently, Nusselt number, entropy generation rate, and Bejan number increase with Pr.

Acknowledgements The authors (A. Tamayol and M. Bahrami) gratefully acknowledge the financial support of the Natural Sciences and Engineering Research Council of Canada (NSERC).

References

Ali, M.E.: On thermal boundary layer on a power-law stretched surface with suction or injection. Int. J. Heat Fluid Flow **16**, 280–290 (1995)

Al-Odat, M.Q., Damesh, R.A., Al-Azab, T.A.: Thermal boundary layer on an exponentially stretching continuous surface in the presence of magnetic field effect. Int. J. Appl. Mech. Eng. **11**, 289–299 (2006)

Banks, W.H.H.: Similarity solutions of the boundary layer equations for a stretching wall. J. Mecan. Theor. Appl. **2**, 375–392 (1983)

Bejan, A.: Entropy Generation Minimization, the Method of Thermodynamic Optimization of Finite-Size Systems and Finite-Time Processes. CRC Press, Boca Rotan (1995)

Bejan, A., Dincer, I., Lorenteh, S., Reyes, H.: Porous and Complex Flow Structures in Modern Technologies. Springer, New York (2004)

Brinkman, H.: A calculation of the viscous force exerted by a flowing fluid on a dense swarm of particles. Appl. Sci. Res. A **1**, 27–34 (1949)

Cortell, R.: Flow and heat transfer of a fluid through a porous medium over a stretching surface with internal heat generation/absorption and suction/blowing. Fluid Dyn. Res. **37**, 231–245 (2005)

Crane, L.J.: Flow past a stretching plate. J. Appl. Math. Phys. **21**, 645–647 (1970)

Elbashbeshy, E.M.A.: Heat transfer over a stretching surface with variable surface heat flux. J. Phys. D **31**, 1951–1954 (1998)

Elbashbeshy, E.M.A.: Radiation effect on heat transfer over a stretching surface. Can. J. Phys. **78**, 1107–1112 (2000)

Elbashbeshy, E.M.A., Bazid, M.A.: Heat transfer over a continuously moving plate embedded in a non-darcian porous medium. Int. J. Heat Mass Transf. **43**, 3087–3092 (2000)

Elbashbeshy, E.M.A., Bazid, M.A.A.: Heat transfer over a stretching surface with internal heat generation. Appl. Math. Comput. **138**, 239–245 (2003)

Elbashbeshy, E.M.A., Bazid, M.A.A.: Heat transfer over an unsteady stretching surface. Heat Mass Transf. **41**, 1–4 (2004)

Famouri, M., Hooman, K.: Entropy generation for natural convection by heated partitions in a cavity. Int. Commun. Heat Mass Transf. **35**, 492–502 (2008)
Hooman, K.: A superposition approach to study slip-flow forced convection in straight microchannels of arbitrary but uniform cross-section. Int. J. Heat Mass Transf. **51**, 3753–3762 (2008)
Hooman, K., Gurgenci, H.: Effects of viscous dissipation and boundary conditions on forced convection in a channel occupied by a saturated porous medium. Transp. Porous Med. **68**, 301–319 (2007)
Hooman, K., Gurgenci, H., Merrikh, A.A.: Heat transfer and entropy generation optimization of forced convection in porous-saturated ducts of rectangular cross-section. Int. J. Heat Mass Transf. **50**, 2051–2059 (2007)
Ishak, A., Nazar, R., Pop, I.: Unsteady mixed convection boundary layer flow due to a stretching vertical surface. Arabian J. Sci. Eng. **31**, 165–182 (2006)
Kaviany, M.: Principles of Heat Transfer in Porous Media. Springer, New York (1992)
Kiwan, S., Ali, M.E.: Near-slit effects on the flow and heat transfer from a stretching plate in a porous medium. Numer. Heat Transf. A **54**, 93–108 (2008)
Kumari, M., Slaouti, A., Takhar, H.S., Nakamura, S., Nath, G.: Unsteady free convection flow over a continuous moving vertical surface. Acta Mech. **116**, 75–82 (1996)
Magyari, E., Keller, B.: Exact solutions for self-similar boundary-layer flows induced by permeable stretching surfaces. Eur. J. Mech. B **19**, 109–122 (2000)
Mehmood, A., Ali, A., Shah, T.: Heat transfer analysis of unsteady boundary layer flow by homotopy analysis method. Commun. Nonlinear Sci. Numer. Simul. **13**, 902–912 (2008)
Nazar, R., Ishak, A., Pop, I.: Unsteady boundary layer flow over a stretching sheet in a micropolar fluid. Int. J. Math. Phys. Eng. Sci. **2**, 161–165 (2008)
Nield, D.A., Bejan, A.: Convection in Porous Media. Springer, New York (2006)
Nield, D.A., Kuznetsov, A.V.: Forced convection in porous media: transverse heterogeneity effects and thermal development. In: Vafai, K. (ed.) Handbook of Porous Media, 2nd edn, pp. 143–193. Taylor and Francis, New York (2005)
Pantokratoras, A.: Flow adjacent to a stretching permeable sheet in a Darcy-Brinkman porous medium. Transp. Porous Med. **80**, 223–227 (2009)
Sadeghi, E., Bahrami, M., Djilali, N.: Analytical determination of effective thermal conductivity of PEM fuel cell gas diffusion layers. J. Power Sources **179**, 200–208 (2008)
Sakiadis, B.C.: Boundary layer behaviour on continuous solid surfaces:I.boundary layer equations for two-dimensional and axisymmetric flow. AICHE **7**, 26–28 (1961a)
Sakiadis, B.C.: Boundary layer behaviour on continuous solid surfaces:II.boundary layer behaviour on continuous flat surfaces. AICHE **7**, 221–225 (1961b)
Seshadri, R., Sreeshylan, N., Nath, G.: Viscoelastic fluid flow over a continuous stretching surface with mass transfer. Mech. Res. Commun. **22**, 627–633 (1995)
Starov, V.M., Zhdanov, V.G.: Effective viscosity and permeability of porous media. Colloids Surf. A **192**, 363–375 (2001)
Tamayol, A., Bahrami, M.: Analytical determination of viscous permeability of fibrous porous media. Int. J. Heat Mass Transf. **52**, 2407–2414 (2009)
Yu, B., Chiu, H.-T., Ding, Z., Lee, L.J.: Analysis of flow and heat transfer in liquid composite molding. Int. Polym. Process. **15**, 273–283 (2000)